Archives of Toxicology
https://doi.org/10.1007/s00204-020-02659-9

ORGAN TOXICITY AND MECHANISMS

Bilirubin disrupts calcium homeostasis in neonatal hippocampal neurons: a new pathway of neurotoxicity

Rossana Rauti[1,3] · Mohammed Qaisiya[2,4] · Claudio Tiribelli[2] · Laura Ballerini[1] · Cristina Bellarosa[2]

Received: 22 October 2019 / Accepted: 3 February 2020

Abstract

Severe hyperbilirubinemia leads to bilirubin encephalopathy in neonates, causing irreversible neurological sequelae. We investigated the nature of neuronal selective vulnerability to unconjugated bilirubin (UCB) toxicity. The maintenance of intracellular calcium homeostasis is crucial for neuron survival. Calcium release from endoplasmic reticulum (ER) during ER-stress can lead to apoptosis trough the activation of Caspase-12. By live calcium imaging we monitored the generation of calcium signals in dissociated hippocampal neurons and glial cells exposed to increasing UCB concentrations. We showed the ability of UCB to alter intracellular calcium homeostasis, inducing the appearance of repetitive intracellular calcium oscillations. The contribution of intracellular calcium stores and the induction and activation of proteins involved in the apoptotic calcium-dependent signaling were also assessed. Thapsigargin, a specific inhibitor of Sarco/endoplasmic reticulum ATPase (SERCA) pumps, significantly reduced the duration of Ca^{2+} oscillation associated with UCB exposure indicating that UCB strongly interfered with the reticulum calcium stores. On the contrary, in pure astrocyte cultures, spontaneous Ca^{2+} transient duration was not altered by UCB. The protein content of GRP78, AT6, CHOP, Calpain and Caspase-12 of neuronal cells treated with UCB for 24 h was at least twofold higher compared to controls. Calcium-dependent Calpain and Caspase-12 induction by UCB were significantly reduced by 50% and 98%, respectively when cells were pretreated with the ER-stress inhibitor 4-PBA. These results show the strong and direct interference of UCB with neuronal intracellular Ca^{2+} dynamics, suggesting ER Ca^{2+} stores as a primary target of UCB toxicity with the activation of the apoptotic ER-stress-dependent pathway.

Keywords Neuroscience · Kernicterus · Bilirubin neurotoxicity · Calcium imaging · ER Ca^{2+} stores · Apoptotic pathways

Introduction

Elevated level of unconjugated bilirubin (UCB) is responsible for the clinical manifestation of neonatal jaundice. When transient, this phenomenon has no clinical consequences, however prolonged and severe hyperbilirubinemia may lead to accumulation of bilirubin and encephalopathy or to a more severe condition named kernicterus (chronic bilirubin encephalopathy) characterized by irreversible neurological sequelae (Watchko and Tiribelli 2013). This pigment circulates in blood bound to albumin (UCB) with only a minimal free fraction known as free bilirubin (Bf). When the plasma concentration bilirubin is markedly elevated, the Bf can passively cross cell membrane (Zucker et al. 1999) with the central nervous system as the most vulnerable organ (Gazzin et al. 2012). Neurons, and in particular immature ones, are mostly sensitive to UCB toxicity (Falcão et al. 2006; Brito et al. 2008).

Electronic supplementary material The online version of this article (https://doi.org/10.1007/s00204-020-02659-9) contains supplementary material, which is available to authorized users.

✉ Rossana Rauti
rrauti@sissa.it

✉ Cristina Bellarosa
cristina.bellarosa@fegato.it

[1] International School for Advanced Studies (SISSA), Via Bonomea, 265, 34136 Trieste, Italy

[2] Fondazione Italiana Fegato (FIF), Bldg Q-AREA Science Park Basovizza, SS14 Km 163,5, 34149 Trieste, Italy

[3] Present Address: Department of Biomedical Engineering, Tel Aviv University, Tel Aviv, Israel

[4] Present Address: College of Pharmacy and Medical Sciences, Hebron University, West Bank, Hebron, Palestine

Published online: 03 March 2020

Several studies showed the effects of UCB toward plasma membrane, mitochondria, endoplasmic reticulum (ER), calcium homeostasis, redox state and increased cell death by apoptosis (Watchko 2006). The ability of UCB to alter directly, at the molecular level, neuronal intracellular calcium homeostasis potentially triggering apoptosis in a cell autonomous manner has not been experimentally challenged. Besides calcium storage and signaling, a key function of the ER is the folding and processing of newly synthesized membrane and secretory proteins. Impairments of these functions are responsible of a pathological state termed ER stress that will induce apoptosis if ER functioning cannot be restored.

Among the different intracellular pathways involved in UCB neurotoxicity, in the last decade ER-stress was demonstrated to be a key mechanism both in vitro and in vivo (Lai et al. 2007; Calligaris et al. 2009; Oakes and Bend 2010; Barateiro et al. 2012; Qaisiya et al. 2014; Vodret et al. 2017, 2018). Whole genome gene expression analysis of SH-SY5Y cells exposed to UCB appears similar to the one obtained exposing cells to Thapsigargin which causes ER-stress by inhibiting the SERCA ATPase proteins that maintain the high calcium concentration in the ER (Schiavon et al. 2018). Although UCB accumulates in both neuronal and astrocyte cells, we have previously demonstrated, that UCB induces ER stress only in neuronal cells and not in astrocytes (Qaisiya et al. 2017). Cytosolic increase of calcium was already described in different models of UCB neurotoxicity (Brito et al. 2004; Zhang et al. 2010; Liang et al. 2017), however the underlying mechanisms remains partially unknown. In particular, the direct ability of UCB to selectively target neurons and neuronal spatial and temporal control of intracellular free calcium involving the ER storage machinery.

In this study we expose neonatal hippocampal neurons to UCB and monitor single cell and network activity by live calcium imaging. We documented the timing and appearance of intracellular calcium oscillations upon UCB exposure, such episodes are generated by each UCB treated neuron independently from the ongoing synaptic activity. We further show, by pharmacological treatments, western blot and confocal microscopy that UCB induced ER-stress and calcium release from ER with subsequent Calpain accumulation and Caspase-12 activation. Of notice, these effects were not present in glial cells further confirming the different susceptibility to UCB of the two cell types.

Materials and methods

Cell culture preparation

Isolation of primary hippocampal tissue was operated in agreement with the guidance of the National Institutes of Health and with the proper international and institutional standards for the care and use of animals in research (Italian Ministry of Health, in agreement with the EU Recommendation 2007/526/CE). All procedures were approved by the local veterinary authorities and performed in accordance with the Italian law (Decree 26/14) and the UE guidelines (2007/526/CE and 2010/63/UE). The animal use was approved by the Italian Ministry of Health. All efforts were made to reduce the number of animals used and to minimize animal suffering. All the reagents were purchased from Sigma-Aldrich if not otherwise indicated.

Dissociated hippocampal cultures were prepared from postnatal 2–3 days old (P2-P3) Wistar rats as previously reported (Bosi et al. 2015; Rauti et al. 2019).

Cells were plated on control poly-L-ornithine coated-glass coverslips and were incubated at 37 °C, 5% CO_2 in a culture medium consisting of Neurobasal Medium (Gibco), supplemented with B27 (2%; Gibco), Glutamax (10 mM; Gibco), and Gentamycin (500×10^{-9} M; Gibco). Half of the culture medium was renewed 4 days after seeding. Cultures were grown until 8–10 days in vitro (DIV) and then used for experiments (Pampaloni et al. 2018).

Primary glial cultures were isolated from neonatal rat (Wistar) cortices at postnatal day 2–3 (P2 – P3), as previously described (Calegari et al. 1999; Rauti et al. 2016). Cells were dissociated and grown into plastic 150 cm^2 flasks and incubated at 37 °C; 5% CO_2 in culture medium composed of DMEM (Invitrogen), supplemented with 10% fetal bovine serum (FBS; Thermo Fisher), 100 IU/mL penicillin, and 10 mg/mL streptomycin. After 3 weeks, glial cells were incubated for 5 min with a 10% trypsin/EDTA solution, detached from the flask and then plated on poly-L-ornithine (Sigma) coated coverslips (Kindler, EU) at a concentration of 50,000 cells in a volume of 200 µL.

Treatments

UCB toxicity is related to the amount of the free bilirubin (Bf) (Ahlfors et al. 2009) and the threshold value of toxicity in vitro occurs at Bf of 70 nM (Ostrow et al. 2003). Three different Bf concentration were tested: 40 nM, 90 nM and 140 nM. Bilirubin (Sigma-Aldrich) was purified as previously described (McDonagh and Assisi 1972), dissolved in DMSO (3 µg/µL) and added to cell medium or to recording solution in the presence of BSA 30 µM. The concentration of total bilirubin necessary to reach the desired Bf concentration (40 nM, 90 nM and 140 nM) in the presence of BSA 30 µM was calculated according to Roca et al. (Roca et al. 2006). Accordingly, control experiments were performed exposing the cells to an equal amount of DMSO.

Phenylbutyric acid (4-PBA, Sigma-Aldrich) was prepared by titrating equimolecular amount of 4-PBA with sodium hydroxide to pH 7.4. Cells were pretreated with 2 mM of

4-PBA for 2 h and then treated with DMSO or UCB at the indicated Bf for additional 24 h in the presence of 4-PBA.

Thapsigargin (Santa Cruz) and carbonyl cyanide 3-chlorophenylhydrazone (Sigma-Aldrich) were dissolved in DMSO. TTX (Latoxan) was dissolved in water (1 mM).

Live cell imaging

Neuronal and glial cells were incubated in 4 µM Oregon Green 488 BAPTA-1 AM (Invitrogen) for 40 min (37 °C; 5% CO_2) (Bosi et al. 2015; Rauti et al. 2016). The samples were then placed in a recording chamber mounted on an inverted microscope (Nikon Eclipse Ti-U) where they were continuously perfused at RT by a recording solution of the following composition (mM): 150 NaCl, 4 KCl, 1 $MgCl_2$, 2 $CaCl_2$, 10 HEPES, 10 glucose (pH adjusted to 7.4 with NaOH). Ca^{2+}-free solution was identical to the recording solution except for (in mM): 0 CaCl2, 3 MgCl2, 5 EGTA.

Cultures were visualized with a 20× objective (0.45 NA) and recordings were performed from visual fields (680 × 680 µm^2, binning 4). Neuronal and glial cells positively stained by Ca^{2+} dye Oregon green 488 BAPTA-1 were simultaneously visualized within the sampled area and on average 30 ± 10 fluorescent cells were measured in each field.

Ca^{2+}-dye was excited at 488 nm with a mercury lamp; excitation light was separated from the light emitted from the sample using a 395 nm dichroic mirror and ND filter (1/8). Images were continuously acquired (exposure time 150 ms) using an ORCA-Flash4.0 V2 sCMOS camera (Hamamatsu). The imaging system was controlled by an integrating imaging software (HCImage Live). All the drugs were diluted with recording solution at the following concentrations (in µM): 1 TTX, 2 carbonyl cyanide 3-chlorophenylhydrazone (CCCP), 5 thapsigargin.

Recorded images were analyzed off-line with Fiji (selecting ROIs around cell bodies), Clampfit software (pClamp suite, 10.2 version; Molecular Devices LLC, US) and Igor Pro Software (6.32 A version; WaveMetrics, Lake Oswego, Oregon, USA).

Intracellular Ca^{2+} transients were expressed as fractional amplitude increase ($\Delta F/F_0$, where F_0 is the baseline fluorescence level and ΔF is the rise over baseline); we determine the onset time of neuronal activation by detecting those events in the fluorescence signal that exceed at least five times the standard deviation of the noise. Oscillation duration was defined as the time from the beginning of the calcium rise over the baseline to the time when the amplitude declined to the baseline. Hence, after obtaining the average values from each cell in a visual field, data were pooled for all the samples recorded under the same experimental conditions and averaged for further comparison.

Western blot

Total proteins were extracted by lysing the cells in ice-cold cell lysis buffer (Cell Signaling Technology, USA). Protein concentration was determined by the bicinchoninic acid protein assay (BCA) according to manufacturer's instructions. Equal amounts of protein were separated by 12% SDS-polyacrylamide gel electrophoresis (SDS-PAGE) and transferred to PVDF membranes (Bio-Rad Laboratories). Membranes were blocked in 5% milk or 4% BSA in T-TBS (0.2% Tween 20, 20 mM Tris–HCl (pH 7.5) and 500 mM NaCl) and incubated overnight at 4 °C with primary antibodies: anti GRP78 (Santa Cruz Biotechnology, sc-13968), anti ATF-6α (Santa Cruz Biotechnology, sc-166659), anti GADD153 (CHOP) (Gene Tex, GTX112827), anti Calpain (Santa Cruz Biotechnology, sc-30064), anti CASP12 (Elab Science, E-AB-64000), anti β-Tubulin (Santa Cruz Biotechnology, sc-32293)) and anti Actin (Sigma-Aldrich, A 2066). Membranes were then incubated with anti-rabbit (Dacko Laboratories, Dako-p0448) or anti-mouse HRP-conjugated secondary antibody (Dacko Laboratories, Dako-p0260). Protein bands were detected by peroxide reaction using ECL Plus Western Blot detection system solutions (ECL Plus Western Blot detection reagents, GE-Healthcare Bio-Sciences). The relative intensities of protein bands were scanned and analyzed using the C-DiGit® Blot Scanner—LI-COR (Biosciences). The optical density of the the bands of interest were normalized to actin or β-tubulin and represented as relative to DMSO-treated cells. Data are the mean ± SD of four independent experiments.

Immunocytochemistry

Cultured hippocampal neurons (two cultures; 9–10 DIV) were incubated with Bf 90 nM for 24 h. Cultures were then fixed by 4% formaldehyde in PBS for 20 min at RT and blocked and permeabilized in 5% fetal bovine serum (FBS), 0.3% Triton-X 100 in PBS for 30 min at RT. Samples were incubated with primary antibodies anti Calpain (Santa Cruz Biotechnology, sc-30064), 1:500 dilution; anti CASP12 (Elab Science, E-AB-64000), 1:250 dilution; anti-β-tubulin III (Sigma, T2200), 1:500 dilution) diluted in PBS with 5% FBS for 45 min. Cultures were then incubated with secondary antibodies (Alexa 488 goat antimouse (Invitrogen, A32723), 1:500 dilution; Alexa 594 goat antirabbit (Invitrogen, A32740), 1:500 dilution) and DAPI to stain the nuclei for 45 min at RT and finally mounted on 1 mm thick glass coverslips using the Fluoromont mounting medium (Sigma). Images were acquired using a Nikon C2 Confocal, equipped with Ar/Kr, He/Ne, and UV lasers. Images were acquired with a 20× (NA) and 40× (NA) objective. Confocal sections were acquired every 0.5 µm and identical binning, gains, and exposure times were used for all images of the

same marker. Image analysis was performed using Volocity software (Volocity 3D image analysis software, PerkinElmer, USA). Each Z-stack was collapsed into a maximum intensity projection image, prior to intensity analysis. For fluorescence intensity analysis of caspase 12 and Calpain, a mask was created enclosing the entire neuron. The threshold for creating the mask was determined based on average and SD values for every image (Ahmad et al. 2018).

Statistical analysis

All data are presented as mean ± standard deviation (SD) of the mean. A statistically significant difference between two data sets was assessed by Student's *t* test for parametric data. Differences between different groups were assessed using two-way ANOVA and multiple comparisons, adjusted by Bonferroni or Holm–Sidak correction. Statistical significance was determined at $p < 0.05$, unless otherwise indicated. Significance was graphically indicated as follows: $*p < 0.05$, $**p < 0.01$, $***p < 0.001$.

Results

UCB affects Ca^{2+} transients

To investigate the ability of UCB to impact neuronal calcium dynamics in functional networks, dissociated hippocampal neurons were treated with different concentrations of free bilirubin (see methods) and the emerging effect was explored by live calcium imaging.

Neurons, stained with the membrane permeable Ca^{2+} dye Oregon Green 488 BAPTA-1 AM, were simultaneously visualized within the sampled area (visual field 680 × 680 μm^2; Fig. 1a, left panel); an of average 30 ± 4 fluorescent cells were isolated and imaged in each visual field. Calcium activity was assessed before and after bilirubin exposure. Calcium dynamics did not differ in saline solution among the different samples, that were pooled together and collectively named Control.

In Fig. 1a (right panel) sample tracings of spontaneous fluorescent recordings (left traces) or bilirubin-induced (right traces) at the three different concentrations (40 nM, 90 nM, and 140 nM Bf), respectively. UCB significantly ($**p < 0.01$) increased the duration of Ca^{2+} waves (42 ± 6 s, $n = 150$ cells, Bf 40 nM; 54 ± 8 s, $n = 140$ cells, Bf 90 nM; 50 ± 8 s, $n = 155$ cells, Bf 140 nM; $n = 5$ samples for each condition from three different series of cultures) when compared to controls (7 ± 3 s, $n = 450$ cells, $n = 15$ samples, from three different series of cultures; see the histogram plot in Fig. 1a, bottom panel). Bilirubin-induced Ca dynamics are reversible. 5 min washout did not affected the Ca++ dynamics brought about by 10 min bilirubin application, for all concentrations tested (Bf 40 nM: from 42 ± 6 to 37 ± 10 s, after 5 min removal, $n = 5$ cells; Bf 90 nM: from 54 ± 8 to 51 ± 8 s, after 5 min removal, $n = 5$ cells; Bf 140 nM: from 50 ± 6 to 42 ± 8 s, after 5 min removal, $n = 4$ cells). Conversely, upon 10 min bilirubin washout, a decrease in the Ca++ events' duration was detected (Bf 40 nM: 11 ± 10 s, $n = 5$ cells; Bf 90 nM: 22 ± 8 s, $n = 5$ cells; Bf 140 nM: 27 ± 8 s, $n = 5$ cells), suggestive of a progressive clearance of bilirubin, with the Ca++ event duration resembling that of controls (See supplementary Fig. 1S).

Since we detected similar effects of the three different UCB concentrations, in the next set of experiments we selected 90 nM Bf as the concentration for subsequent experiments. Hippocampal cultured neurons once reorganized ex vivo develop functional synaptic circuits characterized by the generation of electrical activity. We next investigated whether the effect of UCB in changing calcium oscillations depended on the generation and propagation of action potentials. Figure 1b shows that application (≥ 5 min) of Tetrodotoxin (TTX, 1 µM; a blocker of fast voltage-dependent Na^+ channels) fully blocked the spontaneous bursts of activity (middle trace) but did not block the calcium oscillations induced by UCB application, as this treatment had only a slight effect on the duration of the Ca^{2+} oscillations, significantly ($**p < 0.01$) higher when compared before (8 ± 3 s, $n = 120$ cells, $n = 4$ samples, from two different series of cultures) and after (44 ± 10 s, $n = 120$ cells, $n = 4$ samples, from two different series of cultures) UCB perfusion.

These results point to the ability of UCB to impact calcium pathways although do not allow to distinguish whether the effect is at the extracellular or intracellular level.

Intracellular calcium dependence of UCB calcium signals

To explore the nature of the observed oscillatory pattern induced by UCB, we investigated its dependence on extracellular and intracellular calcium. As shown in Fig. 2a, when cultures were superfused with a calcium-free solution, these events showed only a slight, not significant, reduction in their duration when compared to UCB application (40 ± 8 vs. 50 ± 10 s, $n = 120$ cells, $n = 4$ samples from two series of cultures) but a significant ($**p < 0.01$) increase when compared to the control (8 ± 3 s, $n = 120$ cells, $n = 4$ samples from two series of cultures). Remarkably, the impact of UCB on calcium oscillations is not dependent on the absence of external calcium.

We then explored the possible contribution of intracellular Ca^{2+} sources, starting from the role of mitochondrial Ca^{2+} uptake by the use of mitochondrial protonophore carbonyl cyanide 3-chlorophenylhydrazone (CCCP) which dissipates the proton gradient across the inner mitochondrial membrane and disrupts Ca^{2+} uptake (Fabbro et al. 2007).

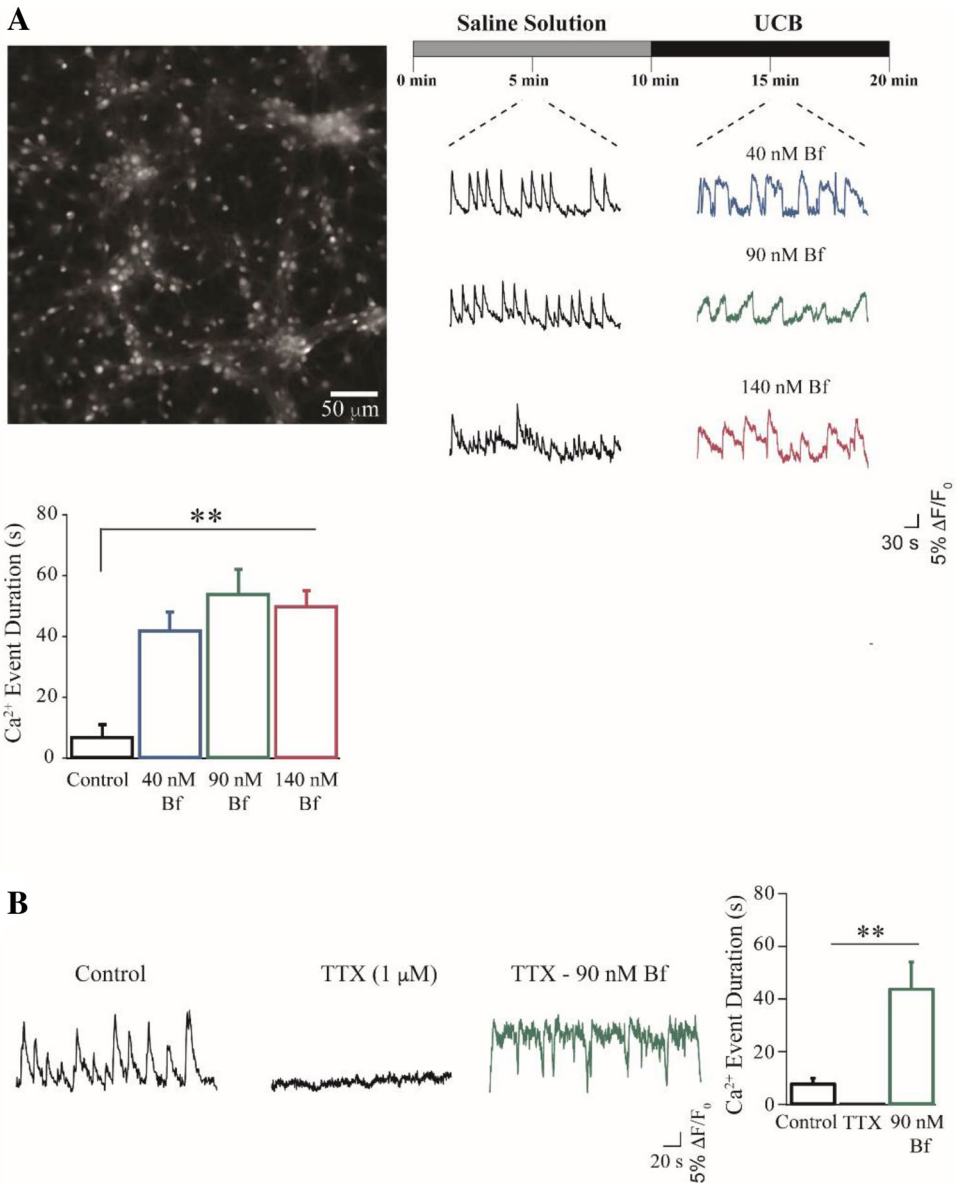

Fig. 1 UCB impact on Ca^{2+} signaling in hippocampal neuronal cultures. **a** Snapshot of representative filed of neuronal cultures stained with the Oregon Green 488-Bapta-1 AM calcium indicator; repetitive Ca^{2+} events spontaneously (left) or UCB-induced (right) at the three different concentrations, recorded in hippocampal cultures; histogram of the average of Ca^{2+} oscillation duration in normal saline solution and id UCB Bf 40 nM, 90 nM and 140 nM, respectively (**$p < 0.01$; multiple comparisons two-way ANOVA test). **b** Repetitive Ca^{2+} fluorescence recordings in saline solution, TTX (1 µM) and in the presence of UCB Bf 90 nM; histogram reporting the duration of Ca^{2+} in the three different conditions (**$p < 0.01$; multiple comparisons two-way ANOVA test)

Figure 2b shows that CCCP treatment (2 µM; 3–7 min) caused a slight, not significant reduction (in the Ca^{2+} oscillations induced by UCB application (38 ± 6 vs. 44 ± 6 s, $n = 120$ cells, $n = 4$ samples from two series of cultures). Conversely, their duration was significantly (**$p < 0.01$) higher compared to the control condition (10 ± 2 s, $n = 120$ cells, $n = 4$ samples from two series of cultures)

Another source of calcium store and release derives from the endoplasmic reticulum (ER). Thapsigargin (5 µM; 10 min), a specific inhibitor of sarco/endoplasmic reticulum ATPase (SERCA) pumps, greatly affected the ability of UCB to impact neuronal Ca^{2+} activity (Fig. 2c) by reducing the duration of Ca^{2+} oscillation induced by UCB (16 ± 4 vs 51 ± 8 s, respectively, $p < 0.01$, $n = 110$ cells, $n = 4$ samples from two series of cultures).

UCB does not impact on Ca^{2+} transients in glial cells.

To investigate if UCB has exclusively the ability to impair neuronal network, pure glial cells cultures were grown for 3 weeks and calcium imaging recordings were performed with or without UCB, at the three different concentrations. Figure 3a, left-panel, shows a representative visual field of glial cells loaded with the Ca^{2+} permeable dye and on the left panel, representative fluorescent tracings of glial cells before and after UCB perfusion, at the three different concentrations. Contrary to what observed in neurons, UCB at the three concentrations tested has no effect on Ca^{2+} oscillation durations comparing control cultures (Fig. 3b). Surprisingly, UCB has no impact on Ca^{2+} oscillation durations comparing control cultures (18 ± 4 s, $n = 60$ cells, $n = 2$ samples

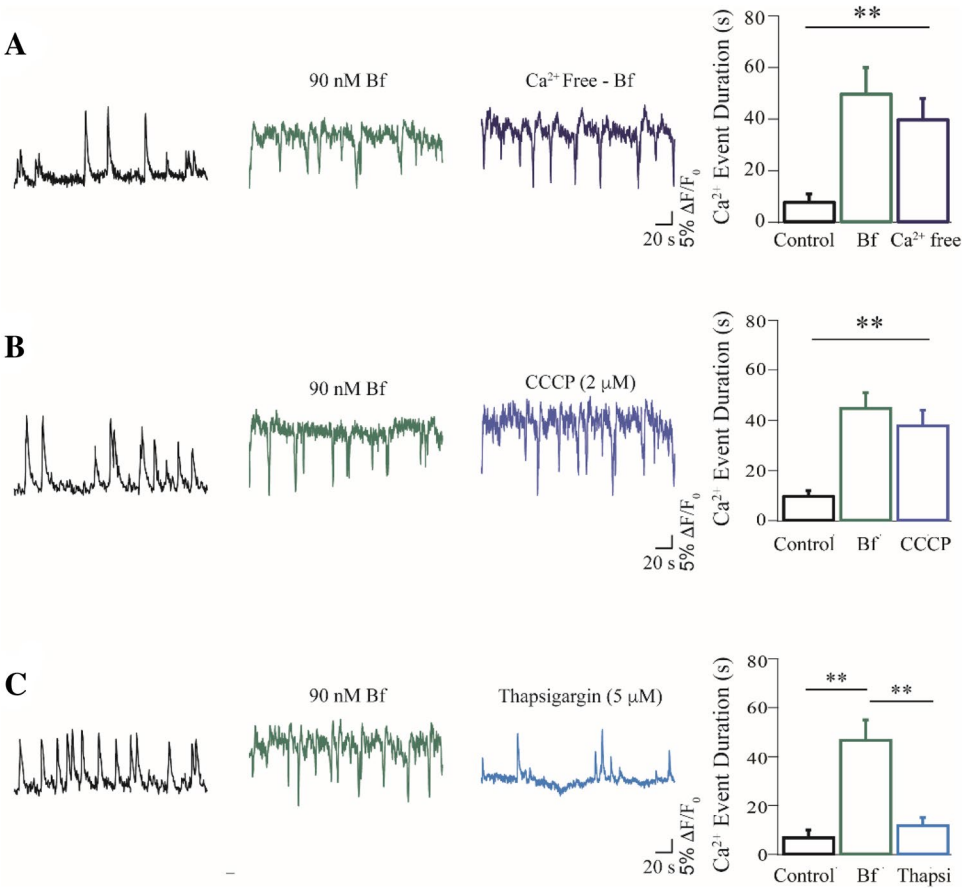

Fig. 2 UCB effect on intracellular Ca^{2+} sources. **a** Repetitive Ca^{2+} fluorescence recordings in saline solution, 90 nM Bf, and in the absence of extracellular calcium; histogram reporting the duration of Ca^{2+} in the three different conditions (**$p < 0.01$; multiple comparisons two-way ANOVA test). **b** Repetitive Ca^{2+} fluorescence recordings in saline solution, 90 nM Bf, and in the presence of CCCP (2 μM); histogram reporting the duration of Ca^{2+} in the three different conditions (**$p < 0.01$; multiple comparisons two-way ANOVA test). **c** Repetitive Ca^{2+} fluorescence recordings in saline solution, 90 nM Bf, and in the presence of Thapsigargin (5 μM); histogram reporting the duration of Ca^{2+} in the three different conditions (**$p < 0.01$; multiple comparisons two-way ANOVA test)

from two series of cultures), with Bf 40 nM (24 ± 5 s, $n = 58$ cells, $n = 2$ samples from two series of cultures), Bf 90 nM(18 ± 6 s, $n = 60$ cells, $n = 2$ samples from two series of cultures), and Bf 140 nM(22 ± 6 s, $n = 58$ cells, $n = 2$ samples from two series of cultures; see plot in Fig. 3b).

UCB induces the expression of proteins involved in calcium-dependent apoptotic signaling

ER function as a dynamic Ca^{2+} store and has a very high Ca^{2+} level compared to cytosol. When ER calcium stores are depleted, the unfolded protein response (UPR) is activated and when prolonged, it leads to apoptosis. We analyzed the protein expression of ER stress-related genes and of the proteins involved in calcium-dependent apoptotic signaling in the neuronal cells exposed to Bf 90 nM for 24 h. Compared to DMSO-treated cells, neuronal cells treated with UCB showed an induction of GRP78 (1.9 ± 0.8-fold, $p < 0.05$), cleaved p50 ATF6 (2.1 ± 0.9-fold, $p < 0.05$) and CHOP (2.7 ± 1.4-fold, $p < 0.01$). Neuronal cells treated with UCB showed also an up-regulation of Calpain (1.95 ± 0.9-fold, $p < 0.05$) and the activation of the cleaved Caspase-12 (5.4 ± 1.5-fold, $p < 0.01$) (Fig. 4a, b).

Caspase-12 and Calpain activation were also investigated in neuronal cultures treated with UCB Bf 90 nM for 24 h, by immunofluorescence staining, co-immunolabeling the cytoskeletal neuronal component β-tubulin III (Fig. 5). UCB induced a significant (**$p < 0.01$ increase in Caspase 12 intensity (176 ± 20%, $n = 7$ visual fields, from two series of cultures), compared to control sister cultures ($n = 7$ visual fields, from two series of cultures; see bar plot in Fig. 5a). Similarly, Bf 90 nM promoted a significant (**$p < 0.01$; $n = 7$ visual fields, from two series of cultures; Fig. 5b) increase in Calpain intensity (216 ± 25%; $n = 7$ visual fields, from two series of cultures) compared to control sister cultures (see bar plot in Fig. 5b).

ER stress inhibition reduces Calpain and cleaved Caspase-12 induction by UCB

A severe and prolonged ER-stress causes cell death. To study the effect of ER-stress on the activation of calcium-dependent Calpain/Caspase-12 signaling, cells were treated with UCB in the presence of 4-PBA, a pharmacological chaperone promoting ER folding/trafficking, commonly considered as an ER-stress inhibitor. Compared to cells treated with Bf 90 nM in the absence of 4-PBA, the presence of 4-PBA

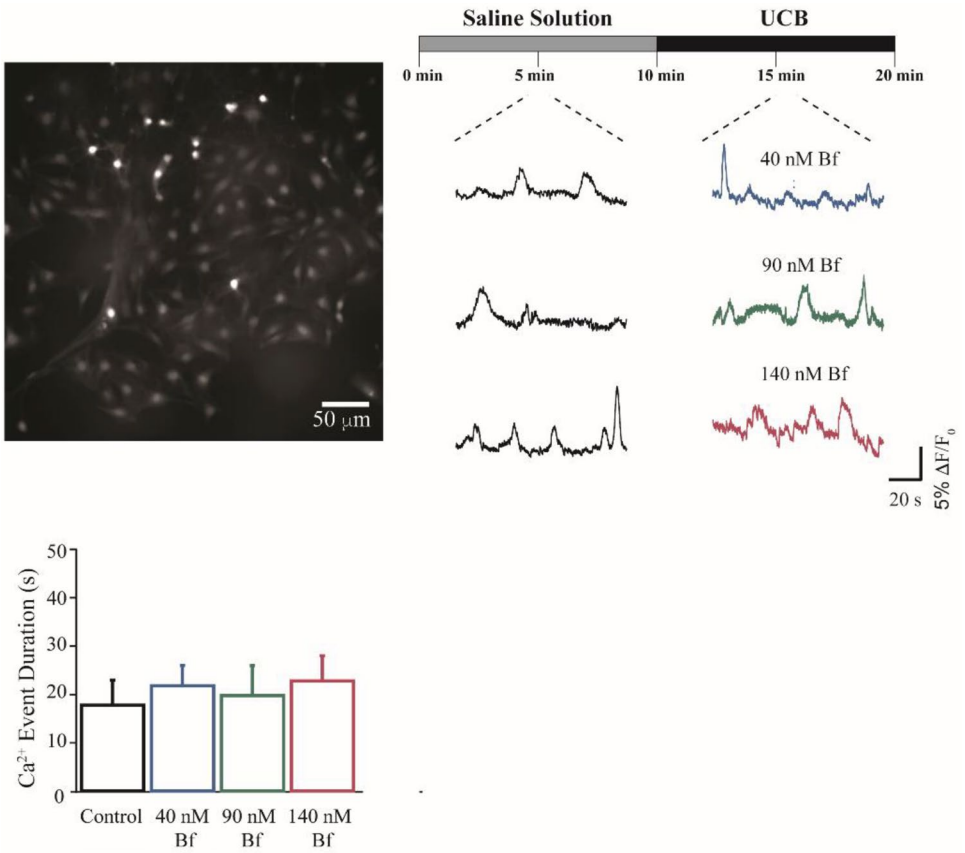

Fig. 3 UCB doesn't impact on Ca^{2+} signaling in glial hippocampal cultures. **a** Snapshot of representative filed of glial cultures stained with the Oregon Green 488-Bapta-1 AM calcium indicator; repetitive Ca^{2+} events spontaneously (left) or UCB-induced (right) at the three different concentrations, recorded in hippocampal glial cultures; histogram of the average of Ca^{2+} oscillation duration in normal saline solution and id UCB Bf 40 nM, 90 nM and 140 nM, respectively

showed a 55% (*$p < 0.05$) and 97% (**$p < 0.001$) downregulation in the induction of Calpain and cleaved Caspase-12, respectively (Fig. 4c, d).

Discussion

The exposure of neurons to UCB in vitro is associated with the perturbation of intracellular calcium homeostasis (Brito et al. 2004; Zhang et al. 2010; Liang et al. 2017) and increased death by apoptosis (Watchko and Tiribelli 2013). UCB damage seems to affect several vital functions rather than a single cell death pathway (Ostrow et al. 2004) and UCB induced cell death is not linked to a single pathway. In addition to the role of mitochondria in mediating apoptotic cell death initiated by UCB (Rodrigues et al. 2002), the activation of caspase 8, an initiator of apoptosis, was described (Seubert et al. 2002) as the participation of NMDA receptors, along with the bilirubin-induced inhibition of protein kinase C activity (Grojean et al. 2000).

Here we investigated the ability of UCB to activate the cell signaling that leads to apoptosis starting from ER-stress, involving ER calcium release, Calpain increase and Caspase-12 activation (Lai et al. 2007). For the first time, the impact of bilirubin in neuronal cultures was assessed by taking advantage of the live-cell calcium technique, an important tool able to provide highly qualitative and quantitative information regarding intracellular mechanisms involving calcium signaling (Grienberger and Konnerth 2012).

The main finding is the novel demonstration that bilirubin has the ability to strongly impact the complex pattern of Ca^{2+} signaling in neuronal cultures. Dissociated hippocampal cultures allow direct experimental access to nervous microcircuits. This preparation has been used in neuroscience research for a long time (Rauti et al. 2016; Lovat et al. 2005) and represents a useful model for studying the dynamics of brain neurotoxicity (Shah et al. 1997; Silva et al. 2006). Our study shows that the application of bilirubin results into larger repetitive Ca^{2+} oscillations, whose generation and spreading do not depend on action potential and thus synaptic activity (Fabbro et al. 2007) (Fig. 1). Calcium is a key player of cell fate and regulates the activity of several proteins. Cells regulate the intracellular calcium through integrated channels located on plasma membrane, mitochondria and ER. We observed that blocking Ca^{2+} reuptake at the level of ER consistently suppressed oscillations led by UCB and suggested that UCB operate on the endoplasmic reticulum calcium sources (Fig. 2). The ER plays a central role in cellular calcium storage, signaling and in the folding and

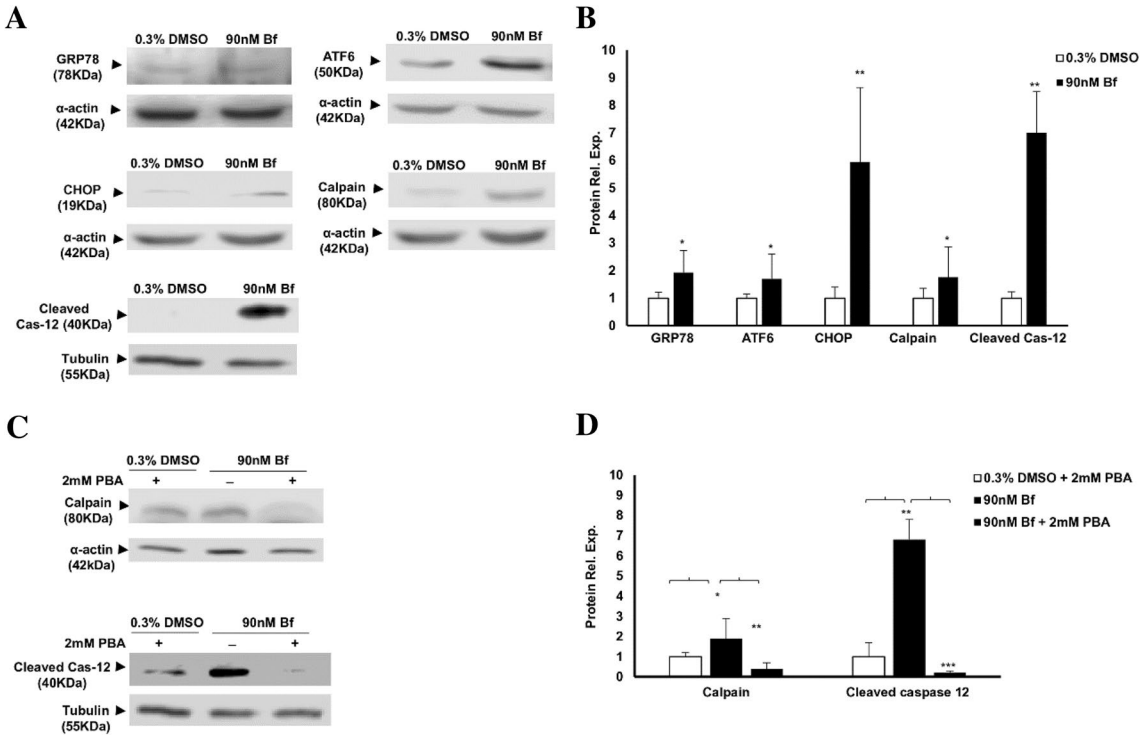

Fig. 4 Effect of UCB treatment on proteins involved in calcium-dependent apoptotic signaling in the presence or absence of ER stress inhibitor (4-PBA). **a** Representative Western Blot for of GRP78, ATF6, CHOP, Calpain and cleaved Caspase-12 in neuronal cells treated with 0.3% DMSO and Bf 90 nM for 24 h. **b** The optical density of each band was normalized to Actin or β-Tubulin and represented as relative to cells treated with DMSO. **c** Representative Western Blot for Calpain and Cleaved Caspase-12 in neuronal cells exposed to 0.3% DMSO or 90 nM Bf for 24 h in the presence (+) or absence (−) of 4-PBA. **d** The optical density of the the bands of Calpain and cleaved Caspase-12 were normalized to Actin or β-Tubulin and represented as relative to DMSO-treated cells. Data are the mean ± SD of at least three independent experiments (*$p < 0.05$, **$p < 0.01$; Student *t* test)

processing of newly synthesized membrane and secretory protein. These calcium-dependent processes require high calcium activity for correct functioning (Verkhratsky 2005). When ER calcium stores are depleted, the unfolded protein response (UPR) is activated initially to reestablish normal ER function. When the stress is severe and prolonged, ER-stress induces cell death (Mekahli et al. 2011). Under ER stress the genetic program activated involves both genes like grp78 that make cells resistant to the stressful conditions (Kaufman 1999) and genes like gadd153 (CHOP) a major player in ER stress-induced apoptosis (Oyadomari and Mori 2004). ER-resident Caspase-12 is also involved in the execution of ER stress-induced apoptosis (Nakagawa et al. 2000). Calpains, a family of Ca^{2+}-dependent cysteine proteases, have been shown to play a role in Caspase-12 activation (Nakagawa and Yuan 2000) and elevation of cytoplasmic Ca^{2+} level leads to the accumulation and activation of Calpain at the ER membrane, where it can activate Caspase-12 (Lai et al. 2007).

The evidence that UCB operates on the endoplasmic reticulum calcium sources (Fig. 2) explains well the early ER-stress induction by UCB we have previously observed on SH-SY5Y (Calligaris et al. 2009; Qaisiya et al. 2017). In the present work, we confirmed further the UPR activation by UCB, since we detected protein induction of the ER-resident chaperone GRP78/Bip and of the pro-apoptotic mediator CHOP (Li et al. 2009) after exposure of hippocampal neurons to UCB (Fig. 4a, b). The increase in Ca^{2+} concentration in the cytosol activates Calpain, which cleaves and activates pro Caspase-12. Activated CASPASE 12 cleaves and activates downstream CASPASES 9 and 3 leading to apoptosis (Lai et al. 2007). UCB exposure on hippocampal neurons activates Calpain and Caspase-12 (Figs. 4a, b, 5) and this effect is blunted by 4-PBA (Fig. 4c, d) indicating that this the activation of the apoptotic pathway is mediated by ER-stress induced by UCB.

Of notice is the observation that in astrocytes, the spontaneous glial Ca^{2+} transients duration was not altered by UCB (Fig. 3). This is in line with our previous demonstration that ER-stress does not occur in U87 astrocytoma cell line despite a intracellular UCB accumulation similar to neuronal cells (Qaisiya et al. 2017). This finding may be at the basis of the higher sensitivity of neuronal than glial cells to UCB toxicity (Falcão et al. 2006; Brito et al. 2008).

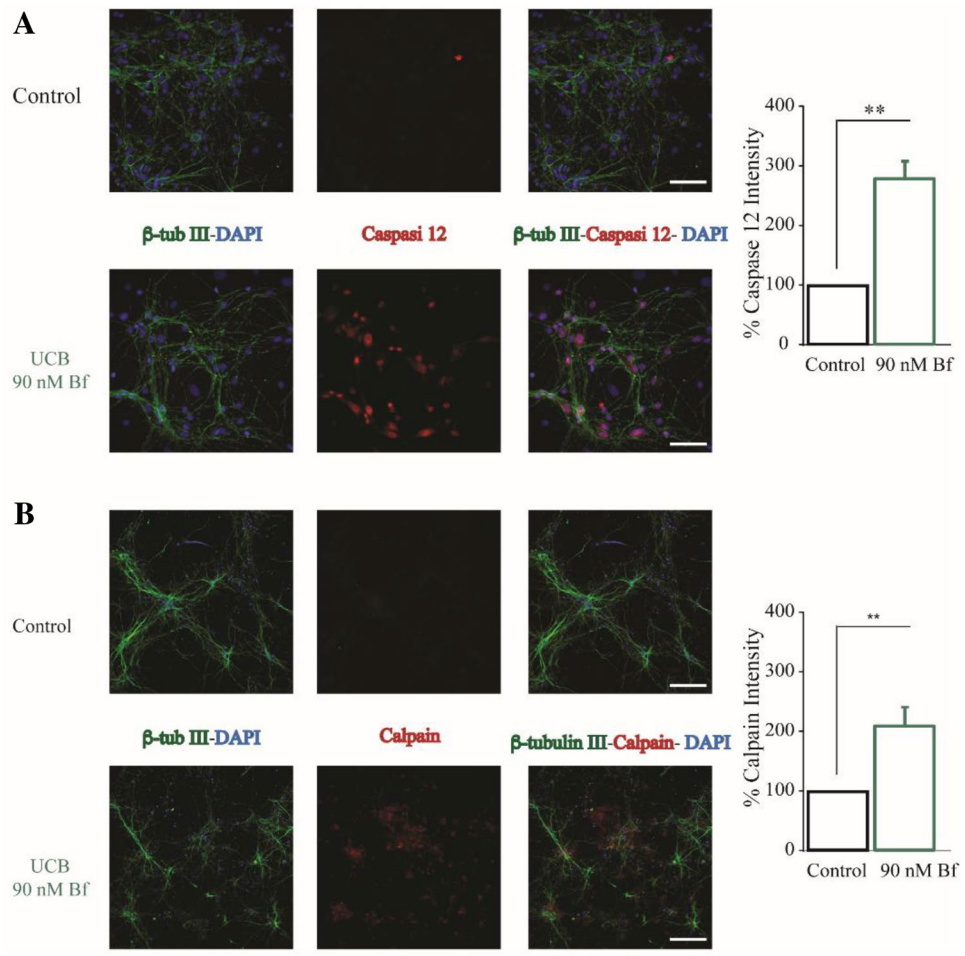

Fig. 5 Caspase-12 and Calpain expression induced by UCB. **a** Confocal microscopic images of two representative fields of hippocampal neuronal cultures grown on control (top) or incubated with UCB 90 nM Bf (bottom). Cells were immune-stained for β-tubulin III to point out neurons (in green, left columns), DAPI for nuclei (in blue, left columns), and Caspase-12 (in red, central columns), and Overlapping of all the three stains (right columns). The percentage of Caspase-12 intensity in the two conditions was evaluated and represented as histogram (**$p < 0.01$; Student *t* test). **b** Confocal microscopic images of two representative fields of hippocampal neuronal cultures grown on control (top) or incubated with UCB 90 nM Bf (bottom). Cells were immune-stained for β-tubulin III (in green, left columns), DAPI for nuclei (in blue, left columns), and Calpain (in red, central columns), and Overlapping of all the three stains (right columns). The percentage of Calpain intensity in the two conditions was evaluated and represented as histogram (**$p < 0.01$; Student *t* test)

Increase intracellular Ca^{2+} events can be both an inducer of ER stress or/and a result of ER-stress. Further studied are needed to understand if UCB acts first directly on ER-membrane Ca^{2+} receptors causing Ca^{2+} release or if induces ER-stress. If ER-stress would be the primary event, the CHOP activation by UCB could be responsible for the Ca^{2+} depletion from ER. CHOP is a pro-apoptotic mediator of ER-stress induced ER oxidase 1α (ERO1α) activates the inositol-1,4,5-trisphosphate receptor (IP_3R), leading to calcium release from ER (Li et al. 2009). The release of Ca^{2+} form ER lumen can contribute significantly to cell death via Calpain/Caspase-12 (Lai et al. 2007; Manié et al. 2014). This hypothesis is sustained also from data collected on glial cells, where CHOP induction and intracellular calcium increase are both absent upon UCB treatment.

The strong and direct interference of UCB with neuronal intracellular Ca^{2+} dynamics can also explain the mechanisms involved in minocycline protection against bilirubin neurotoxicity. Minocycline is a broad-spectrum tetracycline antibiotic and in rat liver minocycline was demonstrated to be a Calcium ions chelator (Antonenko et al. 2010). In the hyperbilirubinemic Gunn Rat model, minocycline administration was demonstrated to prevent cerebellar hypoplasia (Lin et al. 2005), bilirubin-induced neurologic dysfunction (BIND) (Daood et al. 2012) and brainstem auditory evoked potentials (BAEPs) abnormalities (Geiger et al. 2007; Rice et al. 2011). Further investigation are needed to clarify minocycline mechanisms of action.

Conclusions

We have shown a strong and direct interference of UCB with neuronal intracellular Ca^{2+} dynamics, while the calcium homeostasis in glial cells remained undisturbed. Our data suggest the neuronal endoplasmic reticulum but not mitochondrial Ca^{2+} stores as a primary target of UCB. This induces the expression of ER-stress related proteins and the activation of the cytosolic calcium-dependent apoptosis pathway (Fig. 6). These results may be relevant to understand the early events and a better treatment of bilirubin-induced neurological damage and to prevent the permanent neurological damages caused by kernicterus.

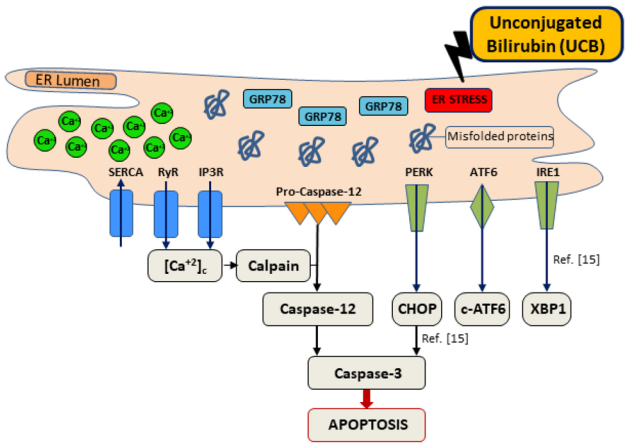

Fig. 6 Proposed pathophysiology of UCB on neuronal cell calcium dynamics and downstream effects. Our data suggest the neuronal endoplasmic reticulum Ca^{2+} stores as a primary target of UCB. This induces the expression of ER-stress related proteins and the activation of the cytosolic calcium-dependent apoptosis pathway involving Calpain induction and Caspase 12 activation

Acknowledgements We thank FIF technician Sandra Leal for the purification of the amount of bilirubin needed to perform calcium imaging experiments. This work was supported in part by an intramural grant of Fondazione Italiana Fegato and by Taawon "Zamala Program" (Mohammed Qaisiya fellowship).

Compliance with ethical standards

Conflict of interest The authors report no conflicts of interest.

References

Ahlfors CE, Wennberg RP, Ostrow JD, Tiribelli C (2009) Unbound (free) bilirubin: improving the paradigm for evaluating neonatal jaundice. Clin Chem 55(7):1288–1299

Ahmad F, Das D, Kommaddi RP, Diwakar L, Gowaikar R, Rupanagudi KV et al (2018) Isoform-specific hyperactivation of calpain-2 occurs presymptomatically at the synapse in Alzheimer's disease mice and correlates with memory deficits in human subjects. Sci Rep 8(1):13119

Antonenko YN, Rokitskaya TI, Cooper AJL, Krasnikov BF (2010) Minocycline chelates Ca^{2+}, binds to membranes, and depolarizes mitochondria by formation of Ca^{2+}-dependent ion channels. J Bioenerg Biomembr 42(2):151–163

Barateiro A, Vaz AR, Silva SL, Fernandes A, Brites D (2012) ER stress, mitochondrial dysfunction and calpain/JNK activation are involved in oligodendrocyte precursor cell death by unconjugated bilirubin. Neuromolecular Med 14(4):285–302

Bosi S, Rauti R, Laishram J, Turco A, Lonardoni D, Nieus T et al (2015) From 2D to 3D: novel nanostructured scaffolds to investigate signalling in reconstructed neuronal networks. Sci Rep 5:9562

Brito MA, Brites D, Butterfield DA (2004) A link between hyperbilirubinemia, oxidative stress and injury to neocortical synaptosomes. Brain Res 1026(1):33–43

Brito MA, Rosa AI, Falcão AS, Fernandes A, Silva RFM, Butterfield DA et al (2008) Unconjugated bilirubin differentially affects the redox status of neuronal and astroglial cells. Neurobiol Dis 29(1):30–40

Calegari F, Coco S, Taverna E, Bassetti M, Verderio C, Corradi N et al (1999) A regulated secretory pathway in cultured hippocampal astrocytes. J Biol Chem 274(32):22539–22547

Calligaris R, Bellarosa C, Foti R, Roncaglia P, Giraudi P, Krmac H et al (2009) A transcriptome analysis identifies molecular effectors of unconjugated bilirubin in human neuroblastoma SH-SY5Y cells. BMC Genomics 10:543

Daood MJ, Hoyson M, Watchko JF (2012) Lipid peroxidation is not the primary mechanism of bilirubin-induced neurologic dysfunction in jaundiced Gunn rat pups. Pediatr Res 72(5):455–459

Fabbro A, Pastore B, Nistri A, Ballerini L (2007) Activity-independent intracellular Ca^{2+} oscillations are spontaneously generated by ventral spinal neurons during development in vitro. Cell Calcium 41(4):317–329

Falcão AS, Fernandes A, Brito MA, Silva RFM, Brites D (2006) Bilirubin-induced immunostimulant effects and toxicity vary with neural cell type and maturation state. Acta Neuropathol 112(1):95–105

Gazzin S, Zelenka J, Zdrahalova L, Konickova R, Zabetta CC, Giraudi PJ et al (2012) Bilirubin accumulation and Cyp mRNA expression in selected brain regions of jaundiced Gunn rat pups. Pediatr Res 71(6):653–660

Geiger AS, Rice AC, Shapiro SM (2007) Minocycline blocks acute bilirubin-induced neurological dysfunction in jaundiced Gunn rats. Neonatology 92(4):219–226

Grienberger C, Konnerth A (2012) Imaging calcium in neurons. Neuron 73(5):862–885

Grojean S, Koziel V, Vert P, Daval JL (2000) Bilirubin induces apoptosis via activation of NMDA receptors in developing rat brain neurons. Exp Neurol 166(2):334–341

Kaufman RJ (1999) Stress signaling from the lumen of the endoplasmic reticulum: coordination of gene transcriptional and translational controls. Genes Dev 13(10):1211–1233

Lai E, Teodoro T, Volchuk A (2007) Endoplasmic reticulum stress: signaling the unfolded protein response. Physiology 22:193–201

Li G, Mongillo M, Chin K-T, Harding H, Ron D, Marks AR et al (2009) Role of ERO1-alpha-mediated stimulation of inositol 1,4,5-triphosphate receptor activity in endoplasmic reticulum stress-induced apoptosis. J Cell Biol 186(6):783–792

Liang M, Yin X-L, Shi H-B, Li C-Y, Li X-Y, Song N-Y, et al (2017) Bilirubin augments Ca^{2+} load of developing bushy neurons by targeting specific subtype of voltage-gated calcium channels. Sci Rep 7. https://www.ncbi.nlm.nih.gov/pmc/articles/PMC5427978/

Lin S, Wei X, Bales KR, Paul ABC, Ma Z, Yan G et al (2005) Minocycline blocks bilirubin neurotoxicity and prevents hyperbilirubinemia-induced cerebellar hypoplasia in the Gunn rat. Eur J Neurosci 22(1):21–27

Lovat V, Pantarotto D, Lagostena L, Cacciari B, Grandolfo M, Righi M et al (2005) Carbon nanotube substrates boost neuronal electrical signaling. Nano Lett 5(6):1107–1110

Manié SN, Lebeau J, Chevet E (2014) Cellular mechanisms of endoplasmic reticulum stress signaling in health and disease. 3. Orchestrating the unfolded protein response in oncogenesis: an update. Am J Physiol Cell Physiol 307(10):C901–907

McDonagh AF, Assisi F (1972) The ready isomerization of bilirubin IX-in aqueous solution. Biochem J 129(3):797–800

Mekahli D, Bultynck G, Parys JB, De Smedt H, Missiaen L (2011) Endoplasmic-reticulum calcium depletion and disease. Cold Spring Harb Perspect Biol 3(6):a004317

Nakagawa T, Yuan J (2000) Cross-talk between two cysteine protease families. Activation of caspase-12 by calpain in apoptosis. J Cell Biol 150(4):887–894

Nakagawa T, Zhu H, Morishima N, Li E, Xu J, Yankner BA et al (2000) Caspase-12 mediates endoplasmic-reticulum-specific apoptosis and cytotoxicity by amyloid-beta. Nature 403(6765):98–103

Oakes GH, Bend JR (2010) Global changes in gene regulation demonstrate that unconjugated bilirubin is able to upregulate and activate select components of the endoplasmic reticulum stress response pathway. J Biochem Mol Toxicol 24(2):73–88

Ostrow JD, Pascolo L, Tiribelli C (2003) Reassessment of the unbound concentrations of unconjugated bilirubin in relation to neurotoxicity in vitro. Pediatr Res 54(6):926

Ostrow JD, Pascolo L, Brites D, Tiribelli C (2004) Molecular basis of bilirubin-induced neurotoxicity. Trends Mol Med 10(2):65–70

Oyadomari S, Mori M (2004) Roles of CHOP/GADD153 in endoplasmic reticulum stress. Cell Death Differ 11(4):381–389

Pampaloni NP, Lottner M, Giugliano M, Matruglio A, D'Amico F, Prato M et al (2018) Single-layer graphene modulates neuronal communication and augments membrane ion currents. Nat Nanotechnol 13(8):755–764

Qaisiya M, Coda Zabetta CD, Bellarosa C, Tiribelli C (2014) Bilirubin mediated oxidative stress involves antioxidant response activation via Nrf2 pathway. Cell Signal 26(3):512–520

Qaisiya M, Brischetto C, Jašprová J, Vitek L, Tiribelli C, Bellarosa C (2017) Bilirubin-induced ER stress contributes to the inflammatory response and apoptosis in neuronal cells. Arch Toxicol 91(4):1847–1858

Rauti R, Medelin M, Newman L, Vranic S, Reina G, Bianco A et al (2019) Graphene oxide flakes tune excitatory neurotransmission in vivo by targeting hippocampal synapses. Nano Lett 19(5):2858–2870

Rauti R, Lozano N, León V, Scaini D, Musto M, Rago I et al (2016) Graphene oxide nanosheets reshape synaptic function in cultured brain networks. ACS Nano 10(4):4459–4471

Rice AC, Chiou VL, Zuckoff SB, Shapiro SM (2011) Profile of minocycline neuroprotection in bilirubin-induced auditory system dysfunction. Brain Res 1368:290–298

Roca L, Calligaris S, Wennberg RP, Ahlfors CE, Malik SG, Ostrow JD et al (2006) Factors affecting the binding of bilirubin to serum albumins: validation and application of the peroxidase method. Pediatr Res 60(6):724–728

Rodrigues CMP, Solá S, Brites D (2002) Bilirubin induces apoptosis via the mitochondrial pathway in developing rat brain neurons. Hepatology 35(5):1186–1195

Schiavon E, Smalley JL, Newton S, Greig NH, Forsythe ID (2018) Neuroinflammation and ER-stress are key mechanisms of acute bilirubin toxicity and hearing loss in a mouse model. PLoS ONE 13(8):e0201022

Seubert JM, Darmon AJ, El-Kadi AOS, D'Souza SJA, Bend JR (2002) Apoptosis in murine hepatoma hepa 1c1c7 wild-type, C12, and C4 cells mediated by bilirubin. Mol Pharmacol 62(2):257–264

Shah PT, Yoon KW, Xu XM, Broder LD (1997) Apoptosis mediates cell death following traumatic injury in rat hippocampal neurons. Neuroscience 79(4):999–1004

Silva RFM, Falcão AS, Fernandes A, Gordo AC, Brito MA, Brites D (2006) Dissociated primary nerve cell cultures as models for assessment of neurotoxicity. Toxicol Lett 163(1):1–9

Verkhratsky A (2005) Physiology and pathophysiology of the calcium store in the endoplasmic reticulum of neurons. Physiol Rev 85(1):201–279

Vodret S, Bortolussi G, Jašprová J, Vitek L, Muro AF (2017) Inflammatory signature of cerebellar neurodegeneration during neonatal hyperbilirubinemia in Ugt1 (−/−) mouse model. J Neuroinflamm 14(1):64

Vodret S, Bortolussi G, Iaconcig A, Martinelli E, Tiribelli C, Muro AF (2018) Attenuation of neuro-inflammation improves survival and neurodegeneration in a mouse model of severe neonatal hyperbilirubinemia. Brain Behav Immun 70:166–178

Watchko JF (2006) Kernicterus and the molecular mechanisms of bilirubin-induced CNS injury in newborns. Neuromolecular Med 8(4):513–529

Watchko JF, Tiribelli C (2013) Bilirubin-induced neurologic damage—mechanisms and management approaches. N Engl J Med 369(21):2021–2030

Zhang B, Yang X, Gao X (2010) Taurine protects against bilirubin-induced neurotoxicity in vitro. Brain Res 1320:159–167

Zucker SD, Goessling W, Hoppin AG (1999) Unconjugated bilirubin exhibits spontaneous diffusion through model lipid bilayers and native hepatocyte membranes. J Biol Chem 274(16):10852–10862